Journal of the Korean Physical Society, Vol. 67, No. 1, July 2015, pp. 224∼231

Design Optimization of a Small-animal SPECT System Using LGSO Continuous Crystals and Micro Parallel-hole Collimators

Joong Hyun Kim
Center for Ionizing Radiation, Division of Metrology for Quality of Life, Korea Research Institute of Standards and Science, Daejeon 305-340, Korea

Mikiko Ito and Soo Mee Kim
Department of Nuclear Medicine, Seoul National University College of Medicine, Seoul 110-744, Korea

Seong Jong Hong
Department of Radiological Science, Eulji University, Seongnam 461-713, Korea

Jae Sung Lee*
Department of Nuclear Medicine and Biomedical Sciences and Institute of Radiation Medicine, Medical Research Center, Seoul National University College of Medicine, Seoul 110-744, Korea

(Received 8 December 2014, in final form 9 March 2015)

A small-animal single photon emission computed tomography (SPECT) system having compact size and low cost was designed using monolithic LGSO scintillation crystals and micro parallel-hole collimators through Monte Carlo simulations. A spatial resolution of ∼1 mm and a sensitivity of ∼100 cps/MBq were achieved with a four-head SPECT system. A hot rod with a diameter of 1.0 mm was resolved in the SPECT image of the ultra-micro hot spot phantom. Using a thin monolithic crystal and micro collimator, we achieved high spatial resolution and high sensitivity.

PACS numbers: 87.58.Ce, 87.53.Vb, 07.85.-m
Keywords: Animal single photon emission computed tomography, Monte Carlo simulation, LGSO, Small-animal imaging
DOI: 10.3938/jkps.67.224

I. INTRODUCTION

Nuclear medicine imaging techniques provide the spatiotemporal biodistribution of radiolabeled molecular imaging probes related to various diagnostic information for a wide range of disease statuses [1]. In addition, pre-clinical molecular imaging methods based on nuclear medicine technologies play important roles in various areas, such as the development of new drugs and radiopharmaceuticals. Small-animal-dedicated single photon emission computed tomography (SPECT) systems with fine spatial resolution and high sensitivity are now widely used and are regarded as the most important types of *in-vivo* molecular imaging tools [1,2]. In particular, small-animal SPECT systems allow the acquisition of rodent images with finer spatial resolution than small-animal positron emission tomography systems that have intrinsically limited spatial resolutions originating from the positron range and non-collinear photon annihilation [3, 4].

Iodine-125 (I-125) is a widely used radioisotope in nuclear medicine. However, its application is limited to in-vitro radioimmunoassays, anti-body studies and autoradiography because I-125 emits low-energy photons (X-rays and gamma rays with energy less than 35.5 keV) [5,6]. Accordingly, clinical SPECT systems with a high signal trigger threshold usually cannot use I-125.

Currently available commercial pre-clinical SPECT systems mainly use pinhole collimators to achieve a high magnification factor and fine spatial resolution (as good as ∼0.35 mm). However, the high magnification factor requires large-area scintillation cameras and close proximity between the imaging object and the pinhole collimator, resulting in a bulky and expensive SPECT system with a limited scan field of view. Low sensitivity is another disadvantage of the pinhole collimator, but has been overcome by using multiple detector heads and multiple pinholes [7,8].

In this study, we designed a small-animal SPECT system with compact size, sufficiently large field of view,

*E-mail: jaes@snu.ac.kr; Fax: +82-2-745-2938

Table 1. Major properties of NaI(Tl) and $L_{0.9}$GSO crystal's are listed. The LGSO crystal has a higher density and a shorter decay time than the NaI(Tl) crystal and is not hydroscopic. However, the photon yield of LGSO is lower than that of NaI(Tl).

Property	NaI(Tl)	$L_{0.9}$GSO
Density (g/cm^3)	3.67	7.3
Decay time (nsec)	230	41
Photon yield (per keV)	38	23
Hydroscopic	Yes	No
Peak emission (nm)	410	420
Intrinsic activity	No	Yes (Lu-176)

low cost and reasonable sensitivity and spatial resolution. A parallel-hole collimator with micro architecture was adopted for this system. Because the magnification factor of the parallel-hole collimator is 1, a large-area scintillation camera is not required to obtain a sufficient field of view. Reasonable system performance can be achieved by using the micro architecture of the parallel-hole collimator. In this study, we performed a Monte Carlo simulation using the Geant4 application for tomographic emission (GATE) simulation code to optimize the design of the proposed SPECT system [9,10].

II. MATERIALS AND METHODS

1. Optimization of the Intrinsic Performance

The intrinsic performance of a gamma camera is mainly determined by the scintillation crystal and the photomultiplier tube (PMT). For the readout of scintillation light, we selected an H9500 PMT (Hamamatsu Photonics K.K., Japan), which is a position-sensitive multi-anode flat-panel PMT that has the advantages of compact size, large effective area, and small pixel size. The effective area of the H9500 is 49 mm × 49 mm. A total of 256 anodes are arranged in a 16 × 16 array. The size of each anode is 2.8 mm × 2.8 mm, and the pitch between neighboring anodes is 3.04 mm [11]. The anodes have a thickness of 0.1 mm and are covered by glass of 1.5 mm in thickness.

An $L_{0.9}$GSO scintillation crystal was selected to optimize the SPECT performance. LGSO has a high density of ~7.3 g/cm^3 and is a non-hydroscopic crystal. However, LGSO has a lower light output than NaI(Tl) and yields an intrinsic radioactivity from Lu-176. The intrinsic performance of LGSO-based detectors is compared with the intrinsic performances of NaI(Tl)-based detectors in this study. The major properties of these crystals are listed in Table 1.

To optimize the intrinsic performance of the crystal, we investigated the crystal thickness and the surface treatments. The crystal's thickness is a dominant factor in determining the intrinsic detection efficiency and the spatial resolution of a scintillation camera. There is a trade-off between efficiency and resolution. A thicker crystal captures more incident radiation but provides worse spatial resolution owing to the wider spread of the optical photons in the crystal.

The crystal surface treatment is another factor that determines the intrinsic performance. A thin monolithic crystal has six surfaces to be treated: two main surfaces with large areas and four narrow surfaces at the sides. The cut surface of the scintillation crystal that has not been mechanically or chemically polished is referred to as "rough as sliced (or rough)". On the rough surface, the standard deviation of the angle between the mean surface and the micro facet of the crystal is higher than that for a polished crystal surface.

We designed the GATE simulation environment as follows: A thin monolithic crystal of 1 or 3 mm in thickness is coupled with the H9500 PMT, and a thin optical grease layer of 0.1 mm is applied between the crystal and the PMT. The other side of the crystal is covered by an optical reflector. The entrance window of the PMT is a monolithic glass layer of 1.5 mm in thickness. Under the glass layer, there are 256 photocathode pixels that have a total area of 2.8 mm × 2.8 mm. The packing fraction of these anode pixels is 89%. The ~11% of optical photons that do not reach the photocathode pixels are absorbed or reflected. In a real situation, approximately 89% of the optical photons have a chance of being converted into electrons at the photocathode pixels, and these electrons are dispersed in a vacuum layer of 2.5 mm in thickness. At the end of the vacuum layer, these electrons reach the first dynodes. However, the photoelectric effect cannot be simulated easily in the GATE Monte Carlo code. For the convenience of simulation, we adopt a second glass layer rather than a vacuum layer and assume that there is no photoelectric effect between the first and second layers. The optical photons disperse again in the second glass layer, and this dispersion is assumed to be similar to the photoelectric effect. The optical photons passing through the second glass layer are absorbed at the end of the second layer, and the number of absorbed photons is recorded for each pixel.

To evaluate the performance of intrinsic properties, we assessed the intrinsic efficiency, spatial resolution and energy resolution, optical photon light output, and displacement error of the radiation interaction position. In all performance evaluations, ideal small-beam sources were used because these evaluations focused on the intrinsic performance. Radiation sources were 140.5 keV in the Tc-99m simulation and 35.5 keV in the I-125 simulation. The highest gamma-ray energy of I-125 is 35.5 keV. The number of absorbed optical photons was recorded for each pixel, and the position of incident radiation was calculated according to a center-of-mass calculation. Eval-

Table 2. Intrinsic performance of the LGSO crystal for eight different conditions. In the case of the rough crystal, the intrinsic energy resolution and efficiency were slightly better than those of the polished crystal; however, the spatial resolution was notably inferior. One-millimeter-thick crystal was inadequate for 140.5-keV photons because of the low detection efficiency. A polished, 3-mm-thick crystal was selected for the SPECT system.

Radiation Energy	Surface Treatment	Crystal Thickness	Intrinsic Energy Resolution (%)	Intrinsic Efficiency (40%, 20%)* (cps/MBq)	Intrinsic Spatial Resolution (mm)
35.5 keV I-125	Rough	1 mm	35.9	79.1	0.90
		3 mm	35.9	80.9	1.07
	Polished	1 mm	36.3	78.0	0.55
		3 mm	36.9	77.6	0.74
140.5 keV Tc-99m	Rough	1 mm	18.4	39.2	0.50
		3 mm	18.6	70.4	0.61
	Polished	1 mm	18.8	38.9	0.36
		3 mm	19.1	67.6	0.54

* Energy windows were 40% for 35.5 keV and 20% for 140.5 keV.

uations were performed for rough and polished surfaces. The standard deviation of the angle between the mean surface and a micro facet (sigma alpha) was 0.1 for the polished surface and 6.0 for the rough surface [6].

The intrinsic efficiency was assessed for two crystal thicknesses and two crystal surface treatments of Tc-99m and I-125. The center of the crystal was irradiated with 10^6 photons. The percentages of valid events in the energy window were calculated. The energy windows were 40% for I-125 and 20% for Tc-99m and differed because the intrinsic energy resolutions were different. The intrinsic efficiencies were reported for each condition.

The crystal was irradiated with 10^4 radiations from the center to the corner of the crystal. The positions of detected radiations were recorded as a 128 × 128 matrix, with the pixel size being 380 μm × 380 μm. For one quadrant, radiations were irradiated from [0.19, 0.19] mm to [24.13, 24.13] mm in steps of 2.66 mm (*i.e.*, [0.19 + 2.66n, 0.19 + 2.66n] for n = 0, 1, ..., 9).

The intrinsic spatial resolution was measured by using a Gaussian fitting of the spatial distribution of the incident radiation and was reported as the full width at half maximum (FWHM) in units of millimeters. The intrinsic energy resolution was assessed as the FWHM of the distribution of the optical light output.

Usually, the position of radiation interaction in a monolithic crystal at an edge or a corner tends to move to the center. This error is referred to as the displacement error. The displacement error was calculated as the distance between the actual irradiated position and calculated interaction position in the image.

2. Optimization of the Collimator Performance

The collimator performance is another decisive factor for the overall performance of the SPECT system. A parallel-hole collimator having micro architecture was designed. The area of the collimator is 52 mm × 52 mm so as to cover the area of the scintillation crystal. The collimator consists of 128 × 128 square holes arranged in a square matrix. The area of each hole is 340 μm × 340 μm, and the pitch between holes is 380 μm. The septal thickness is 40 μm. The collimator material is tungsten.

The collimator's performance was optimized for the collimator length. A trade-off exists between the spatial resolution and the sensitivity of a collimator. A longer collimator yields higher spatial resolution, but lower sensitivity. The collimator length was optimized to yield reasonable resolution and sensitivity in consideration of the intrinsic performance of the crystal.

To optimize the collimator's length, we acquired the projection images of a point source at a distance of 26 mm from the collimator surface for various collimator lengths ranging from 10 to 20 mm. At the end of the collimator, we placed an ideal radiation absorber with 100% absorption efficiency and a spatial resolution of 0 mm because the simulation focused on the collimator's performance. The point source generated 10^7 radiations, and a planar projection image was acquired. The collimator's sensitivity was calculated from the total number of recorded counts in the projection image and the number of generated radiations. The spatial resolution of the collimator was acquired by using a Gaussian fitting of the line profile through the point source in the projection image.

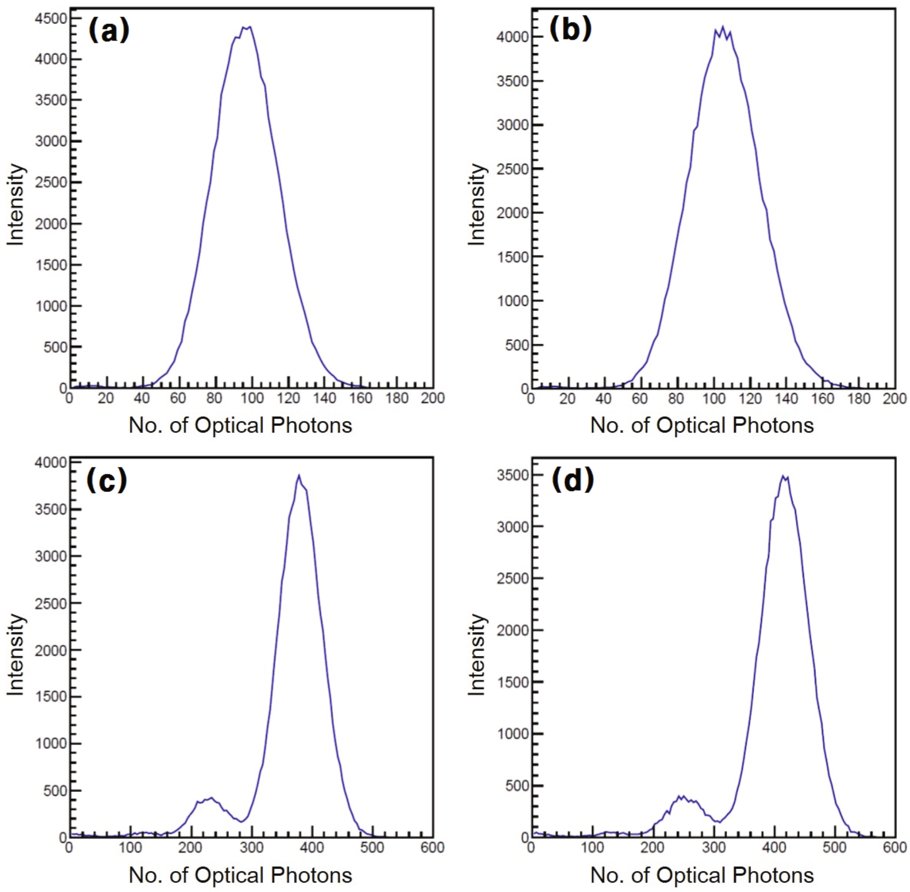

Fig. 1. (Color online) Energy spectra of a 3-mm-thick LGSO crystal; (a) polished surface, 35.5-keV photon, (b) rough surface, 35.5-keV photon, (c) polished surface, 140.5-keV photon, and (d) rough surface, 140.5-keV photon. The energy resolutions of 35.5-keV and 140.5-keV photons were about 36% and 18%, respectively. The light output of the rough surface was higher than that of the polished one.

3. Evaluation of the Intrinsic Activity

The LGSO crystal has intrinsic radioactivity due to the presence of lutetium-176 [12]. The natural abundance of Lu-176 is 2.59% of all lutetium and the half-life of Lu-176 is 3.78×10^{10} years. The calculated Lu-176 activities of 1- and 3-mm-thick crystal are ∼655 and ∼1965 Bq, respectively. The intrinsic radioactivity per square centimeter was measured within two energy windows, 40% for 35.5 keV (I-125) and 20% for 140.5 keV (Tc-99m). The intrinsic radioactivity was compared with a flood source image for radioactivity of 2.5 MBq/cm^2 (67.6 μCi/cm^2), and the background activity level was assessed. To obtain the flood source image, we used the optimized collimator and crystal described above.

4. SPECT Performance

To estimate the performance of the entire SPECT system, we designed a compact four-head SPECT system by using the above optimized collimator and crystal. A field of view of approximately 5 cm in the transaxial and the axial directions can be obtained by using the four-head system. The sensitivity and the planar spatial resolution of the system were assessed according to the intrinsic crystal and collimator performances. To evaluate the spatial resolution of the system, we designed an ultra-micro hot spot phantom (model: ECT/HOT/UMMP, Data Spectrum Corp. NC, USA) by using a GATE simulation. The ultra-micro phantom has a diameter of 2.8 cm and a height of 2.8 cm and consists of six hollow channels having diameters of 0.75, 1.0, 1.35, 1.7, 2.0, and 2.4 mm.

A 100-MBq (2.7-mCi) quantity of I-125 was distributed in the hollow channels of the ultra-micro phantom. The energy spectrum of I-125 was simplified to four photon energies from 27.3 to 35.5 keV with adequate yields. One-hundred twenty projections were acquired in only 2 minutes (4 s for each projection), and the rotation angle was 3 degrees. Projections were reconstructed by using filtered back-projection with a Hanning filter and an ordered-subset expectation maximization with four

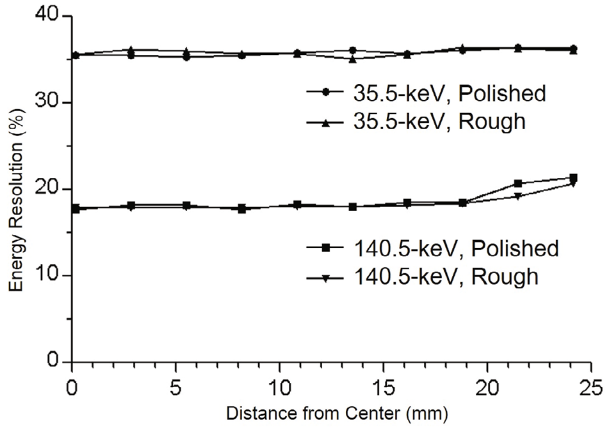

Fig. 2. Energy resolution of a 3-mm-thick LGSO crystal. No notable difference is seen between the polished and the rough surfaces. The energy resolution of 140.5-keV photon is better than that of 35.5-keV photon because of light output difference.

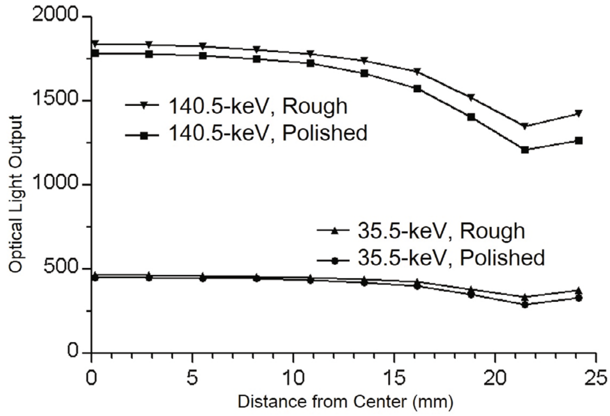

Fig. 3. Optical light output of a 3-mm-thick LGSO crystal. The optical light output of 140.5-keV photon is about 4 times higher than that of 35.5-keV photon because of the energy difference. For the rough surface, the optical light output is slightly higher than the polished one.

subsets and four iterations.

III. RESULTS

1. Intrinsic Performance

The energy spectra of LGSO under the conditions of a polished surface treatment and a crystal thickness of 3 mm are shown in Figure 1. The energy resolutions of I-125 and Tc-99m were approximately 36% and 18%, respectively. Therefore, the intrinsic efficiencies for each isotope were estimated in different energy windows, 40% for I-125 and 20% for Tc-99m. The intrinsic efficiency was mainly determined by the crystal's type and thickness, and not by the crystal's surface treatment. The NaI(Tl) crystal had unacceptable efficiency for the gamma energy of Tc-99m because of its low density. The LGSO crystal, however, had high efficiency. An LGSO crystal with a thickness of only 1 mm yielded perfect efficiency in the entire energy window for I-125. The detection efficiency of I-125 in the 40% energy window for the 1-mm-thick crystal was not notably different from that for the 3-mm-thick crystal. In the case of Tc-99m, the LGSO crystal of 1 mm in thickness had a low detection efficiency ($< 40\%$) whereas the LGSO of 3 mm in thickness had a detection efficiency of approximately 70% in the 20% energy window. Only the LGSO crystal with a thickness of 3 mm was suitable for both I-125 and Tc-99m SPECT imaging.

The energy resolution for Tc-99m was approximately 18%, and there was no notable difference according to the surface treatment. However, the energy resolution worsened as the source position was moved to the edge of the crystal. I-125 had an energy resolution (approximately 36%) twice that of Tc-99m. The trends of the energy

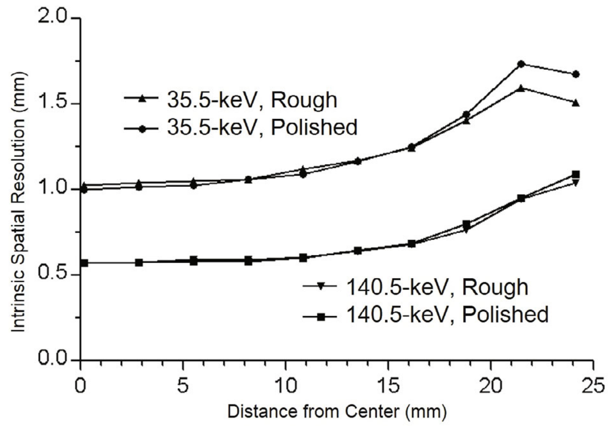

Fig. 4. Intrinsic spatial resolution of a 3-mm-thick LGSO crystal. At the center, the intrinsic spatial resolutions were $\sim$0.55 mm and $\sim$1 mm for 140.5-keV and 35.5-keV photons, respectively. The intrinsic spatial resolution was worse at the edge position than at the center position.

resolution of I-125 were similar to those of Tc-99m in terms of the change in energy resolution with changes in the surface treatment and in the source position (Fig. 2).

The optical light output depended on the surface treatment and the source position (Fig. 3). A rough surface yielded a higher light output than a polished surface (by approximately 3%$-$14% for a 3-mm-thick crystal). The optical light output decreased as the source position was moved to the edge. For the rough surface, the optical light output at the edge was approximately 20%$-$28% lower than that at the center.

The intrinsic spatial resolutions of the 3-mm-thick rough crystal were 0.57-1.04 and 1.03-1.51 mm for Tc-99m and I-125, respectively (Figure 4). When the sources were positioned at the corners of the crystals, the intrinsic spatial resolutions for Tc-99m and I-125 of the 3-mm-thick rough crystal were approximately 5.5%

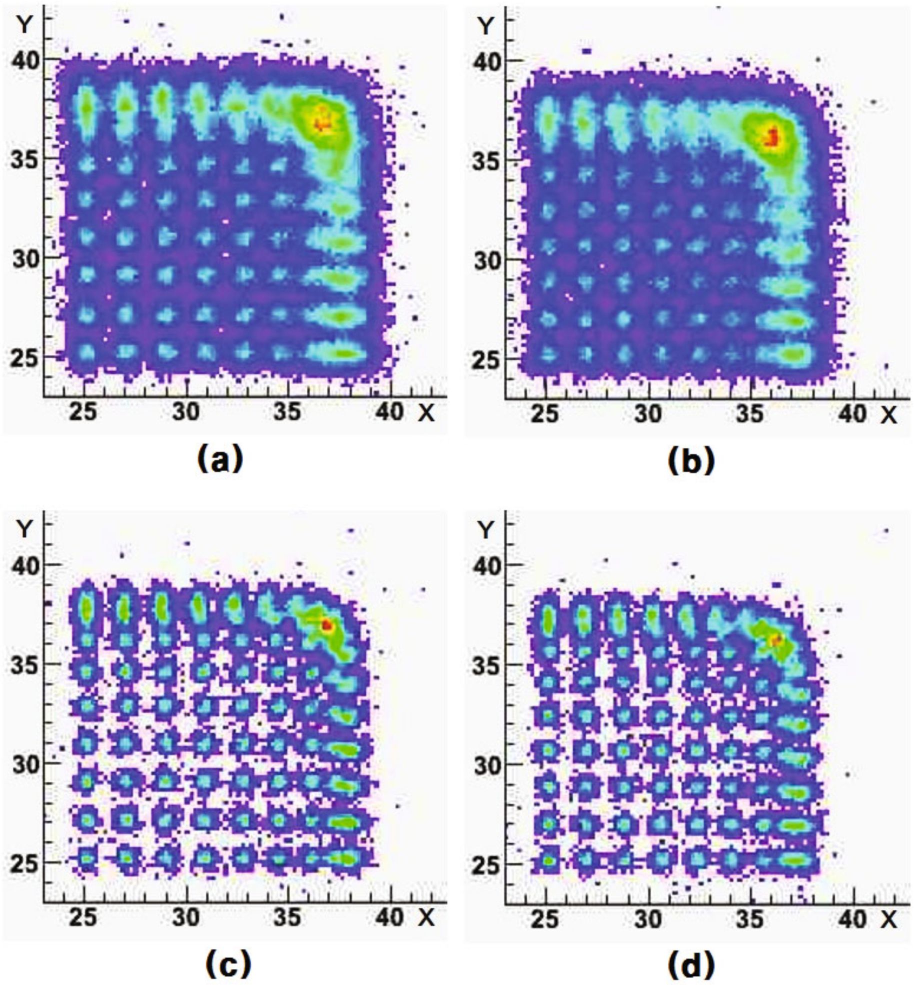

Fig. 5. (Color online) Two-dimensional flood images of a 3-mm-thick LGSO crystal; (a) polished surface, 35.5-keV photon, (b) rough surface, 35.5-keV photon, (c) polished surface, 140.5-keV photon, and (d) rough surface, 140.5-keV photon. The displacement error of the polished crystal at the edge position was smaller than that of the rough crystal.

and 9.9% better than those of the 3-mm-thick polished crystal for respectively.

The displacement error depended on the surface treatment. Two-dimensional flood images are shown in Fig. 5. The polished crystal performed better in distinguishing point sources. The displacement error of the polished crystal was approximately 0.5 mm less than that of the rough crystal for both of Tc-99m and I-125.

2. Collimator Performance

Figures 6(a) and (b) show the sensitivity and the spatial resolution of the collimator versus collimator's length. The collimator's sensitivity decreased from 45.3 to 11.6 cps/MBq as the collimator's length was increased from 10 to 20 mm. The collimator's spatial resolution improved from 0.8 to 0.45 mm as the collimator's length was increased from 10 to 20 mm.

3. Intrinsic Activity

The intrinsic activity induced by Lu-176 was assessed. For a 3-mm-thick crystal, the background activities were 2.33 and 2.75 cps/cm^2 for the Tc-99m and the I-125 energy windows, respectively. With the flood source of 2.5 MBq/cm^2, the detected activities were 79.9 and 107.1 cps/cm^2 for the Tc-99m and the I-125, respectively. The ratios of the background activity to the total count were 2.9% and 2.6% for Tc-99m and I-125, respectively.

4. SPECT Performance

The performances of the entire SPECT system can be estimated from the intrinsic and collimator's performances. The planar spatial resolution of the system was expected to be 1.18 mm for I-125 and 1.05 mm for Tc-99m. The system's sensitivity with four heads was ex-

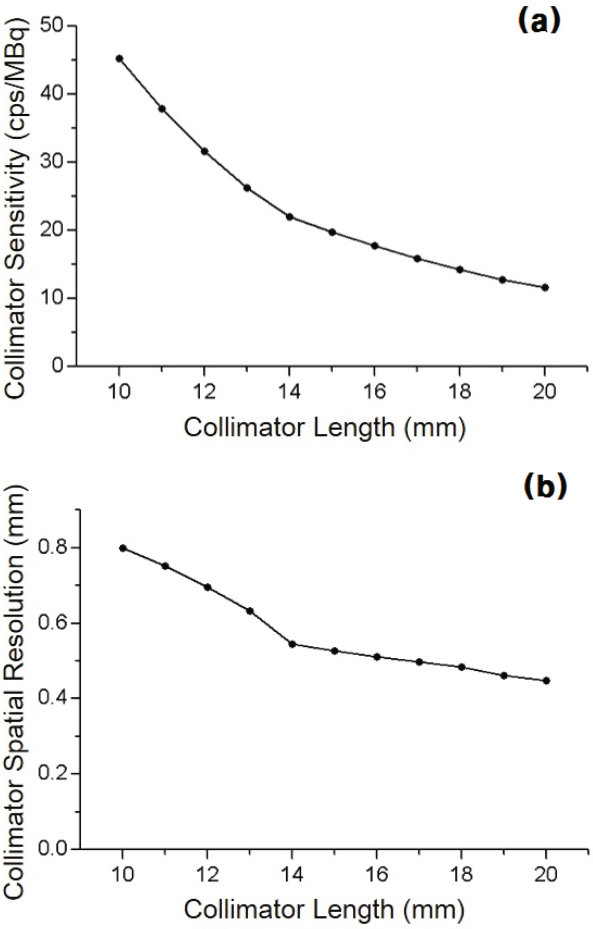

Fig. 6. Results of the collimator's performance according to its length; (a) collimator sensitivity (cps/MBq) and (b) collimator spatial resolution.

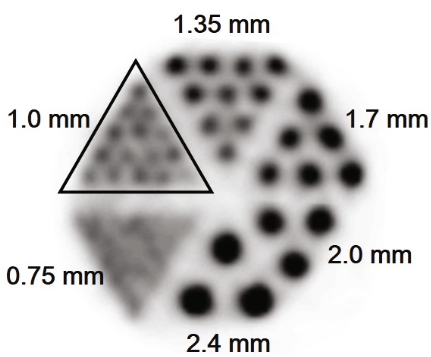

Fig. 7. SPECT image of the ultra-micro hot spot phantom. One hundred twenty planar projection images were reconstructed by using ordered-subset expectation maximization with four subsets and four iterations. Hot spot inserts as small as 1 mm could be resolved.

pected to be 133 cps/MBq for I-125 and 86 cps/MBq for Tc-99m. The micro phantom image reconstructed by using ordered-subset expectation maximization with four subsets and four iterations is shown in Fig. 7. Hot spot inserts as small as 1 mm could be resolved.

IV. DISCUSSION

Commercial micro SPECT systems that are currently available mainly use multi-pinhole collimators to achieve high spatial resolution and high sensitivity. With the pinhole collimator, high spatial resolution can be achieved by using a large-area scintillation crystal and a high magnification factor. However, the gamma camera based on a single-pinhole collimator has unfavorable properties of low sensitivity, a small field of view and resolution degradation at an axially off-center position. A multi-pinhole collimator was proposed to overcome these disadvantages of the single-pinhole collimator.

In this study, a micro SPECT system using a parallel-hole collimator with micro architecture and a thin monolithic crystal was designed. This system provides a sufficiently large field of view for rodent imaging with a much smaller detector than that used in pinhole SPECT systems. The small detector has many advantages. A bench-top micro SPECT system can be developed with a volume of less than 1 m^3 and at reasonable cost. Because only a small amount of scintillation crystal material is required, expensive, but high-quality, crystals can be adopted [13,14]. High sensitivity can be achieved with the parallel-hole collimator. However, the spatial resolution is worse than that of a pinhole collimator. The resolution can be recovered by using an iterative reconstruction with a point spread function or collimator-detector response.

The crystal surface treatment affects the intrinsic properties of the detector. The incident radiation is converted into hundreds to thousands of optical photons in the crystal, and these optical photons travel through the crystal and reach the crystal's surface. At the crystal's surface, optical photons are reflected or absorbed or penetrate the surface. Two different surface treatments can be applied to the two large surfaces of crystals to obtain rough and polished surfaces. No notable differences in the absorption, penetration or reflection were observed for the two surface treatments; however, the uncertainty in the reflection angle differs. We assigned different uncertainty levels for the surfaces (sigma alpha values were 0.1 and 6.0 for polished and rough surfaces, respectively). At the crystal surface, optical photons are reflected if the incidence angle is smaller than the critical angle determined by the reflective indexes of the crystal and the grease. On the polished surface, the angles of incidence and reflection are similar; therefore, the optical photon cannot escape through the large surface if the angle of incidence is smaller than the critical angle. Only optical photons that reach the surface with an angle larger than the critical angle can escape and be detected by the PMT. In the case of the rough surface, however, the angle of reflection is much dispersed after reflection. Therefore, the escape probability for the rough crystal is higher than that for the polished crystal. These properties were reflected in the experimental results for the light output. The light output of the rough crystal was higher than that of the polished crystal.

The energy resolution is related to the optical photon output. A high output yields better energy resolution, and the rough crystal, therefore, yielded better energy resolution than the polished crystal. The intrinsic spatial resolution can also be explained by the sigma alpha value. For the polished crystal, only the optical photons having an angle larger than the critical angle can escape the crystal, and they are detected in the proximal region not far from where the incident radiation is detected. In the rough crystal, however, the escape sites of optical photons are widely dispersed. This explains why the intrinsic spatial resolution of the polished crystal was better than that of the rough crystal.

In this study, we finally selected the 3-mm-thick crystal over the 1-mm-thick crystal. For I-125 imaging, the 1-mm-thick crystal was sufficient. However, the detection of radiation from Tc-99m is more important in SPECT research because Tc-99m is the most widely used isotope in SPECT [15,16]. Although the detection rate of Tc-99m was only 70%, it was measured with a 20% energy window. For a crystal thicker than 3 mm, the detection rate dose not increase, but the spatial resolution degrades. A thickness of 3 mm was, thus, optimal for the SPECT system.

The collimator's length is another important factor that determines the spatial resolution and sensitivity of the system. A long collimator yields a high spatial resolution but low sensitivity. In this study, we selected a collimator length of 15 mm, which provided a spatial resolution of ∼1 mm and a system sensitivity of ∼100 cps/MBq.

V. CONCLUSION

We designed a small-animal SPECT system using a parallel-hole collimator and a thin monolithic crystal. A compact and economic system can be produced on the basis of this design. The SPECT system had a spatial resolution of ∼1 mm and a sensitivity of ∼100 cps/MBq for Tc-99m and I-125 imaging, which is sufficient for the imaging of rodents. The system's performance was verified in an experiment using an ultra-micro hot spot insert phantom.

ACKNOWLEDGMENTS

This work was supported by grants from Seoul National University Hospital (04-2008-0280) and the National Research Foundation of Korea (NRF) funded by the Korean Ministry of Science, ICT and Future Planning (NRF-2014M3C7034000, NRF-2013R1A1A2013175).

REFERENCES

[1] S. Y. Park, H. Yoon, N. Lee, J. K. Oh, I. R. Yoo, S. H. Kim and Y. A. Chung, Nucl. Med. Mol. Imaging. **48**, 272 (2014).
[2] T. K. Lee *et al.*, Nucl. Med. Mol. Imaging. **48**, 225 (2014).
[3] J. R. Stickel and S. R. Cherry, Phys. Med. Biol. **50**, 179 (2005).
[4] M. Rodrìguez-Villafuerte, Y. Yang and S. R. Cherry, Phys. Med. **30**, 76 (2014).
[5] J. Brodfuehrer *et al.*, Pharm. Res. **31**, 635 (2014).
[6] K. H. Yu, H. Yoon, M. G. Song, D. S. Lee and J-K. Chung, Nucl. Med. Mol. Imaging **46**, 239 (2012).
[7] F. Van der Have, B. Vastenhouw, R. M. Ramakers, W. Branderhorst, J. O. Krah, C. Ji, S. G. Staelens and F. J. Beekman, J. Nucl. Med. **50**, 599 (2009).
[8] S. Shokouhi, S. D. Metzler, D. W. Wilson and T. E. Peterson. Phys. Med. Biol. **54**, 207 (2009).
[9] S. Staelens, D. Strul, G. Santin, S. Vandenberghe, M. Koole, Y. D'Asseler, I. Lemahieu and R. Van de Walle, Phys. Med. Biol. **48**, 3021 (2003).
[10] S. Lee, J. Gregor and D. Osborne, Mol. Imaging. **12**, 1 (2013).
[11] S. J. Hong, S. I. Kwon, M. Ito, G. S. Lee, K-S. Sim, K-S. Park, J. T. Rhee and J. S. Lee, IEEE Trans. Nucl. Sci. **55**, 912 (2008).
[12] R. Yao, T. Ma and Y. Shao, Phys. Med. Biol. **53**, 4399 (2008).
[13] M. E. Myronakis and D. G. Darambara, Med. Phys. **38**, 455 (2011).
[14] B. S. McDonald, S. Shokouhi, H. H. Barrett and T. E. Peterson, Nucl. Instrum. Meth. Phys. Res. A **579**, 196 (2007).
[15] H. Choi, W. W. Lee, Y. So, S. Ha, S-S. Byun and S. E. Kim, Nucl. Med. Mol. Imaging **48**, 262 (2014).
[16] M. Lipowska, J. Klenc, R. D. Folks and A. T. Taylor, Nucl. Med. Mol. Imaging **48**, 216 (2014).